

Astrophysically important ^{26}Si states studied with the $(^3\text{He},n)$ reaction and the $^{25}\text{Al}(p,\gamma)^{26}\text{Si}$ reaction rates in explosive hydrogen burning environments

Y. Parpottas,^{1,*} S. M. Grimes,¹ S. Al-Quraishi,^{1,2} C. R. Brune,¹ T. N. Massey,¹ J. E. Oldendick,¹
A. Salas,¹ and R. T. Wheeler¹

¹Ohio University, Athens, Ohio 45701, USA

²Physics Department, King Fahd University of Petroleum and Minerals, Dhahran 31261, Saudi Arabia

(Received 29 September 2004; published 20 December 2004)

Additional experimental information concerning the level structure of ^{26}Si above the proton threshold is needed to reduce uncertainties in the $^{25}\text{Al}(p,\gamma)^{26}\text{Si}$ reaction rate and consequently better determine ^{26}Al radioisotope production in astrophysical environments. The $^{24}\text{Mg}(^3\text{He},n)^{26}\text{Si}$ reaction was measured and excitation energies of states in ^{26}Si were determined with improved accuracy. Spins were assigned to a number of states by comparing their measured differential cross sections with Hauser-Feshbach cross sections. The 3^+ resonance state of the $^{25}\text{Al}(p,\gamma)^{26}\text{Si}$ reaction was identified at 5912(4) keV excitation energy and the $^{25}\text{Al}(p,\gamma)^{26}\text{Si}$ reaction rate in explosive hydrogen burning environments was calculated.

DOI: 10.1103/PhysRevC.70.065805

PACS number(s): 26.30.+k, 25.40.Lw, 25.55.Hp, 27.30.+t

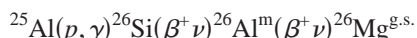
I. INTRODUCTION

The identification of large amounts ($\sim 3M_{\odot}$) [1] of the ^{26}Al radioisotope in the interstellar medium of our galaxy via its decay $^{26}\text{Al}^{\text{g.s.}}(\beta^+\nu)^{26}\text{Mg}^*(E_{\gamma}=1.8\text{ MeV})^{26}\text{Mg}^{\text{g.s.}}$ from spectrometers on satellites [2,3] and recently by CGRO collaboration [1] is of great interest. A comparison of the ^{26}Al half-life ($T_{1/2}=7.2\times 10^5\text{ yr}$) to the time scales of the galactic chemical evolution ($\approx 10^{10}\text{ yr}$) indicated that nucleosynthetic processes are still active in our galaxy [4]. Answers to questions regarding the astrophysical sources of ^{26}Al and the production rate of ^{26}Al in these environments can reveal information about earlier stages in our galaxy related to ^{26}Al sources.

The ^{26}Al production mechanism is dependent on the properties of the astrophysical environment. For example, the ^{26}Al production in nova explosions [5] proceeds as follows:



If the decay of ^{25}Al is bypassed by the proton capture on ^{25}Al at higher temperatures ($T>0.4\text{ GK}$), the resulting reaction sequence



takes place. The $^{25}\text{Al}(p,\gamma)^{26}\text{Si}$ reaction has not yet been measured directly, due to the difficulties of producing a radioactive ^{25}Al beam. At the present time this reaction rate must thus be determined from indirect spectroscopic information. An accurate determination of the $^{25}\text{Al}(p,\gamma)^{26}\text{Si}$ reaction rate remains very important because a quantitative understanding of the ^{26}Al production rate can in turn constrain nova models.

Shell model calculations and mirror nucleus arguments [4] indicate that the $^{25}\text{Al}(p,\gamma)^{26}\text{Si}$ reaction rate in explosive

hydrogen burning environments is probably dominated by a $J^{\pi}=3^+$ ($\ell=0$) resonance state that lies at 5970(100) keV. Additional contributions to the $^{25}\text{Al}(p,\gamma)^{26}\text{Si}$ reaction rates at stellar temperatures of $T<1.5\text{ GK}$ are expected from direct capture and resonances up to 1 MeV above the proton threshold in $^{26}\text{Si}(S_p=5518\text{ keV})$. The compilation of Endt [6] lists the level structure of ^{26}Si above the proton threshold mainly from the results of $^{24}\text{Mg}(^3\text{He},n)^{26}\text{Si}$ [7] and $^{28}\text{Si}(p,t)^{26}\text{Si}$ [8] reaction measurements. Many of these levels still have unknown spin-parity assignments or relatively large ($>20\text{ keV}$) uncertainties in their excitation energies. Recent studies of the $^{28}\text{Si}(p,t)^{26}\text{Si}$ [9] and $^{29}\text{Si}(^3\text{He},^6\text{He})^{26}\text{Si}$ [10] reactions reduced the uncertainties in the ^{26}Si excitation energies for levels above the proton threshold; the first study assigned spin and parity to some states above the proton threshold through distorted-wave Born approximation (DWBA) analysis and the second study assigned J^{π} 's to two new states (1^+ and 3^+) that were not observed in this recent (p,t) [9] measurements. However, more studies are necessary to confirm previous results since even in the two recent high resolution studies [9,10] not all levels just above the proton threshold were observed in each measurement. These levels are expected to play an important role in the astrophysical reaction rates of $^{25}\text{Al}(p,\gamma)^{26}\text{Si}$ which depend sensitively on the excitation energy values.

In this work, the astrophysically important ^{26}Si states were studied via the $^{24}\text{Mg}(^3\text{He},n)^{26}\text{Si}$ reaction. The thin targets, long flight paths, and low bombarding energies provided high resolution for the ^{26}Si states of interest. The $(^3\text{He},n)$ reactions could result in better resolution than the (p,t) or $(^3\text{He},^6\text{He})$ reactions since neutrons could be detected at any distance without losing energy using time-of-flight techniques. The relatively low bombarding energy used in the present experiment has two advantages: the lower neutron energy improves the neutron energy resolution determined by time of flight and the $(^3\text{He},n)$ reaction at low incident energies favors the compound nuclear reaction mechanism, particularly when the outgoing neutron energy is

*Present address: Triangle Universities Nuclear Laboratory, Duke University, Durham, North Carolina 27708-0308.

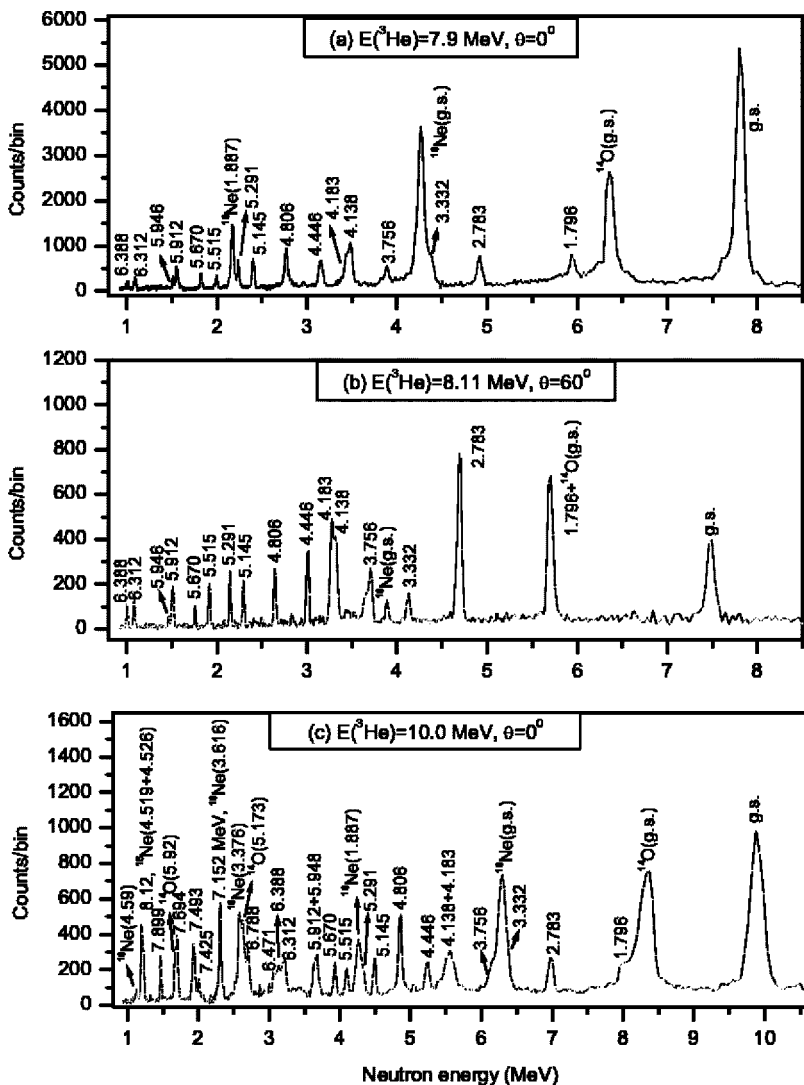


FIG. 1. The neutron-energy spectra of the $^{24}\text{Mg}(^3\text{He},n)^{26}\text{Si}$ reaction measurements. The bin width is given by Eq. (1).

also low (i.e., for high excitation energies of the residual nucleus). On the other hand, the previous experiments which were performed at higher energies (and in some cases involved different reactions) are expected to be dominated by direct reactions which typically only strongly populate natural parity states corresponding to a simple rearrangement of nucleons. The present experiment should be capable of seeing all states regardless of their structure including those with unnatural parity such as the astrophysically important 3^+ state. In many cases it is also possible to assign spins to states lying at high excitation energies by comparing the measured cross section to Hauser-Feshbach calculations.

II. EXPERIMENT

The $^{24}\text{Mg}(^3\text{He},n)^{26}\text{Si}$ reaction was measured at the Ohio University 4.5 MV Van de Graaff Tandem Accelerator. A He^- beam was produced using the duoplasmatron source. It was chopped and bunched at 1.25 MHz, injected into the tandem where it was accelerated and stripped, and eventually a $^3\text{He}^{++}$ pulsed beam was delivered through the swinger magnet to the target with an intensity of 28 pnA.

The $26\text{-}\mu\text{g}/\text{cm}^2$ -thick ^{24}Mg (99.94%) targets were made by evaporation onto 0.2-mm-thick stopping Ta disks. Additional targets were used, such as ^{12}C , Ta_2O_5 , and Ta for identifying contaminants and checking the background, and a thick ^{27}Al for the efficiency measurements. All targets were mounted on a wheel in the scattering chamber. The beam was focused through a 0.64-cm-diameter collimator followed by a 0.32-cm-diameter collimator onto the target located in the center of the scattering chamber. Currents from the scattering chamber, target, and beamstop were summed, integrated, and digitized to determine the number of incident ions. In order to suppress electrons liberated from the collimator at the entrance to the chamber a ring immediately following the collimator was held at a potential of -300 V. A thermoelectric cooler (MI2021T) was used to maintain a cold copper plate a few centimeters from the target, gathering in this way on its surface the contaminant molecules and reducing contamination on a target. The pressure in the scattering chamber was maintained at 10^{-6} torr.

Neutrons were detected in a three-detector array of 12.7-cm-diameter and 5.1-cm-thickness liquid scintillators (two BC501A and one NE213) placed 10 m from the target in the 30-m-long tunnel. Angles were changed by rotating the

TABLE I. Excitation energies (in MeV) and J^π of ^{26}Si states from this work in comparison with previous studies.

| This work | [7] | [9] | [10] | [6] ^f | J^π | [7] ⁱ | [9] | [10] ^j | [6] ^f | [4] ^l |
|---------------------|-----------|------------------------|-----------|-----------------------|-----------------------------|------------------------------------|--|---|-------------------|---|
| 0.0 ^a | 0.0 | 0.0 | 0.0 | 0.0 | 0 ⁺ | 0 ⁺ | 0 ⁺ | 0 ⁺ | 0 ⁺ | 0 ⁺ |
| 1.7959 ^a | 1.800(30) | 1.7959 | 1.7959 | 1.7959(2) | 2 ⁺ ^h | 2 ⁺ | 2 ⁺ ^h | 2 ⁺ | 2 ⁺ | 2 ⁺ |
| 2.7835 ^a | 2.780(30) | 2.7835 | 2.7835 | 2.7835(4) | 2 ⁺ ^h | 2 ⁺ | 2 ⁺ ^h | 2 ⁺ | 2 ⁺ | 2 ⁺ |
| 3.332 ^a | 3.330(30) | 3.330 | — | 3.3325(3) | 0 ⁺ ^h | 0 ⁺ | 0 ⁺ ^h | 0 ⁺ | 0 ⁺ | 0 ⁺ |
| 3.756 ^a | 3.760(30) | 3.756 | — | 3.756(2) | — | — | (3 ⁺) | 3 ⁺ | — | 3 ⁺ |
| — | — | — | — | 3.842(2) ^g | — | — | — | — | — | — |
| — | — | — | — | 4.093(3) ^g | — | — | — | — | — | — |
| 4.138(4) | 4.140(30) | 4.155(2) ^c | 4.144(8) | 4.138(1) | 2 ⁺ | 2 ⁺ | 2 ⁺ ^h | 2 ⁺ | 2 ⁺ | 2 ⁺ |
| 4.183(4) | — | 4.155(2) ^c | 4.211(16) | 4.183(11) | 3 ⁺ | — | (3 ⁺) | 3 ⁺ | — | 4 ⁺ |
| 4.446 ^a | 4.450(30) | 4.445 | 4.446 | 4.446(3) | 2 ⁺ | — | (2 ⁺ +4 ⁺) ⁱ | (2 ⁺ +4 ⁺) | — | 3 ⁺ |
| 4.806 ^a | 4.810(30) | 4.805 | 4.806 | 4.806(2) | (2 ⁺) | 0 ⁺ + (J>0) | (0 ⁺ +2 ⁺ +4 ⁺) ⁱ | (0 ⁺ +2 ⁺ +4 ⁺) | 0 ⁺ | (0 ⁺ , 2 ⁺ , 4 ⁺) |
| 5.145(4) | — | 5.145(2) | 5.140(10) | — | 2 ⁺ | — | 2 ⁺ ⁱ | 2 ⁺ | — | — |
| — | — | — | — | 5.229(12) | — | — | — | — | 2 ⁺ | 2 ⁺ |
| 5.291(4) | 5.310(30) | 5.291(3) | 5.291 | 5.330(20) | 4 ⁺ | 4 ⁺ | 4 ⁺ ^h | 4 ⁺ | 4 ⁺ | 4 ⁺ |
| 5.515(4) | — | 5.515(5) | 5.526(8) | 5.562(28) | 4 ⁺ | — | (4 ⁺) ⁱ | 4 ⁺ | — | 1 ⁺ |
| 5.670(4) | — | — | 5.678(8) | — | 1 ⁺ | — | — | 1 ⁺ ^k | — | — |
| 5.912(4) | 5.910(30) | 5.916(2) | — | — | 3 ⁺ | 0 ⁺ + (4 ⁺) | 0 ⁺ ⁱ | — | — | — |
| 5.946(4) | — | — | 5.945(8) | 5.940(25) | 0 ⁺ | — | — | 3 ⁺ ^k | 0 ⁺ | (0 ⁺ , 4 ⁺) |
| 6.312(4) | 6.320(30) | 6.300(4) ^d | — | — | 2 ⁺ | 2 ⁺ | (L=2) ⁱ | — | — | — |
| 6.388(4) | — | 6.380(4) ^d | — | 6.350(25) | 2 ⁺ | — | (L=2) ⁱ | — | 2 ⁺ | 2 ⁺ |
| 6.471(4) | 6.470(30) | — | — | 6.470(30) | 0 ⁺ | 0 ⁺ | — | — | 0 ⁺ | (1 ⁻) |
| 6.788(4) | 6.780(30) | 6.787(4) | — | 6.789(17) | 3 ⁻ | (2 ⁺) | 3 ⁻ ⁱ | — | 3 ⁻ | (3 ⁻) |
| — ^b | 6.880(30) | — | — | 6.880(30) | — | (0 ⁺) | — | — | (0 ⁺) | (3 ⁻) |
| — | — | 7.019(10) ^e | — | — | — | — | — | — | — | — |
| 7.152(4) | 7.150(30) | 7.160(10) | — | 7.150(13) | 2 ⁺ | 2 ⁺ | 2 ⁺ ^h | — | 2 ⁺ | 2 ⁺ |
| 7.425(4) | 7.390(30) | 7.425(7) | — | 7.390(30) | 0 ⁺ | (0 ⁺) | (L=2) ⁱ | — | (0 ⁺) | — |
| 7.493(4) | 7.480(30) | 7.498(4) | — | 7.489(15) | 2 ⁺ | 2 ⁺ | 2 ⁺ ^h | — | 2 ⁺ | 2 ⁺ |
| 7.694(4) | — | 7.687(22) | — | 7.695(30) | 3 ⁻ | — | 3 ⁻ ⁱ | — | — | — |
| 7.899(4) | 7.900(30) | 7.900(22) | — | 7.892(15) | 1 ⁻ | — | 1 ⁻ ⁱ | — | — | — |

^aThese levels were observed and used for energy calibration.

^bThis level was not observed because of contaminant peaks.

^cAverage centroid of doublet peak.

^dPartially resolved.

^eObserved only in $24^\circ \leq \theta_{c.m.} \leq 37^\circ$ range.

^fCompilation.

^gObserved in a ($^3\text{He}, n\gamma$) reaction [14].

^hFrom Ref. [6].

ⁱFrom DWBA analysis.

^jFrom Ref. [9].

^kFrom mirror nuclei considerations.

^lFrom shell-model calculations and mirror nuclei considerations.

swinger magnet facility [11] around its axis of rotation, keeping the neutron detector array fixed. The adjustable collimators, according to the solid angle (made of polyethylene, lead, and tungsten) at the entrance of the tunnel and the tunnel itself, provided good shielding and background reduction.

A time signal was extracted from the anode signal of the photomultiplier (PMT) bases. Special care was taken to adjust the gain of the PMT bases and the threshold of the constant fraction discriminator (CFD) before sending the signal

to the time-of-flight circuit. These procedures maximized the neutron detector efficiency in the region of interest and rejected unwanted noise without cutting low energy neutrons of interest. Outputs from the CFD corresponding to each detector were sent to the Router and saved. This information was useful in the analysis because it indicated in which neutron detector the event was recorded. An OR CFD output was used as the start signal of the time-to-amplitude converter (TAC) while a beam pickoff signal, after delay by almost a period, was used as the stop signal. The OR outputs of the

pulse shape discrimination and the pulse height circuits were also processed and saved for further analysis. Data were saved in event mode and analyzed off line with cuts on the pulse shape and height optimized for best n - γ discrimination. The dead time of the electronics and the 8-ADC (Analog-to-Digital-Converter) system [12] and also the beam current integration were recorded, in histogram format, for the needs of this analysis too.

Two measurements were taken to study the region just above the proton threshold. Bombarding energies of 7.9 MeV at 0° and 8.11 MeV at 60° were chosen so that the time of flight for the 5.90–5.96 MeV excitation region of ^{26}Si , where the $^{25}\text{Al}(p, \gamma)^{26}\text{Si}$ 3^+ resonance possibly is located, and the 6.31–6.38 MeV previously known doublet in ^{26}Si were close to the maximum practical value, optimizing in this way the energy resolution for these neutron groups. A third measurement was also taken at 10 MeV bombarding energy and 0° to deduce excitation energies up to 7.9 MeV. Each run lasted five days because of the low counting due to the thin targets and the long flight path. The energy calibration and the time resolution were checked every 24 h; the time resolution was 1.5–2.0 ns over the course of the measurements. Three ^{24}Mg targets were utilized in order to minimize any effects of target deterioration and/or carbon buildup. Runs with secondary targets (^{12}C , Ta_2O_5 , and Ta) were also taken under the same kinematic conditions of the three main measurements, for reasons mentioned above.

III. ANALYSIS AND RESULTS

A. Excitation energies of ^{26}Si

The event files were converted into time using the method described in Ref. [13]. The TAC was calibrated using a random spectrum and a calibration circuit which produced pulses separated by a known period. These procedures yield an accuracy in time determination of approximately 1 part in 10^4 . The time spectra, with PSD cuts and dead time corrections for each detector, were added using as reference the ground state and the low excitation levels of ^{26}Si since their excitation energies are accurately known.

The time spectra were rebinned according to neutron energy, using variable-width neutron-energy bins:

$$\Delta E_{bin} = 2fE_n \left[\left(\frac{\Delta x}{x} \right)^2 + \left(\frac{\Delta t}{t} \right)^2 + \left(\frac{\Delta E_b}{E_n} \right)^2 \right]^{1/2}. \quad (1)$$

The following parameters are constants in Eq. (1): $f=0.333$, $\Delta x=0.0254$ m (detector thickness), $x=10$ m (flight path), $\Delta t=1.5$ ns (time resolution), and $\Delta E_b=0.005$ MeV (beam-energy resolution, including the effect of energy loss in the target), while the time of flight t and neutron energy E_n vary over the spectrum. This energy-binning method is not intended to exactly model our neutron-energy resolution, but rather to yield peaks with four to six bins full width at half maximum (FWHM) over the entire spectrum (assuming negligible intrinsic width), using physically reasonable inputs.

The final neutron-energy spectra are presented in Fig. 1. Peak centroids were deduced from fits and converted into excitation energies. The mean beam energy in the target and

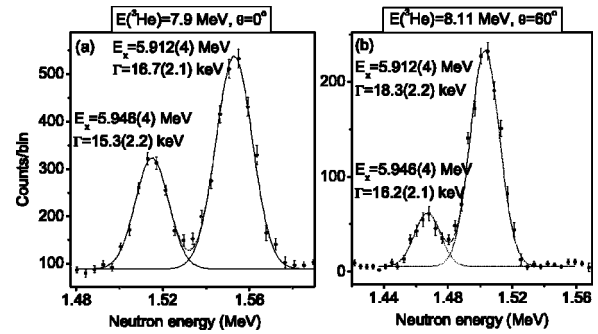


FIG. 2. Neutron-energy spectra fits of the 5.90–5.96 MeV excitation region of ^{26}Si from the low bombarding energy measurements. Excitation-energy centroids and widths (consistent with instrumental resolution) are also shown. The bin width is given by Eq. (1).

the flight path length have been adjusted slightly within their uncertainties in order to optimize the agreement with known low-lying states of ^{26}Si ($E_x < 5$ MeV). The excitation energies derived for these states from our final calibration agreed with known values within ± 3 keV. A 4-keV systematic uncertainty is assigned for states above $E_x=5$ MeV (statistical uncertainties were 1 keV or less). Excitation energy values are labeled in Fig. 1 for each observed level including contaminant peaks due to ^{16}O and ^{12}C . Table I lists the excitation energies of ^{26}Si up to 7.9 MeV from this work in comparison with previous studies. Spin and parity values for these levels are also shown in this table and are discussed in the next section.

Because of the high resolution achieved in this measurement, previously known doublets were partially resolved [4.138–4.183 MeV in Figs. 1(a) and 1(b)] or totally resolved [5.912–5.946 MeV and 6.312–6.388 MeV in Figs. 1(a) and 1(b)]. Also levels at 6.471, 7.152, 7.425, 7.693, and 7.899 MeV were located more accurately (see Table I). Proton-unbound states lying up to 1 MeV above the threshold (the astrophysically important energy range) were seen at 5.670, 5.912, 5.946, 6.312, and 6.388 MeV while in previous studies [7,9,10], two or three of these states were observed (see Table I). The isospin-triplet states of $A=26$ nuclei and $T=1$ given by Endt [6] implies that the $^{25}\text{Al}(p, \gamma)^{26}\text{Si}$ 3^+ resonance should lie in the 5.90–5.96 MeV region. Both members of the previously known doublet [6,7] at 5.90–5.96 MeV excitation region were observed. These states were not seen together in the recent high-resolution measurements; the 5.912 MeV level was reported in the (p, t) work while the 5.945 MeV level in the $(^3\text{He}, ^6\text{He})$ study. These states were resolved in the low bombarding energy measurements where the energy resolution from all contributions was approximately 16 keV at FWHM in that region. The 10-MeV measurement could not separate these levels but one can easily conclude that the broad peak in that region should be a doublet since the observed width is larger than the expected experimental width of nearby states, and it is also asymmetric. Figure 2 shows the neutron-energy spectra of the 5.90–5.96 MeV excitation region of ^{26}Si from the two low bombarding energy measurements. Excitation energies deduced from the neutron peak centroid and width val-

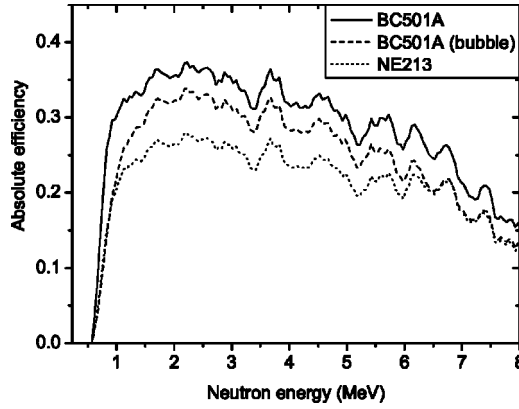


FIG. 3. Neutron detector efficiencies with air and aluminum corrections.

ues from fits are also shown in the figure. No levels seem to have appreciable intrinsic widths since the observed widths and the experimental width values were in agreement within the width error from the fits. This is also in agreement with theoretical calculations of those widths [4] which are of the order of eV ($\Gamma_p + \Gamma_\gamma$).

B. Spin assignments

Since both the 5.912- and 5.946-MeV states were observed, we are able to assign spin to them based on comparison of their differential cross sections with Hauser-Feshbach predicted cross sections. Spins were also assigned to higher excited levels verifying the existing assignments or choosing a specific J^π in the case that more than one J^π was reported by previous studies.

The differential cross section was calculated from the neutron yield according to the following equation:

$$\frac{d\sigma}{d\Omega} = \frac{Y}{I\eta\Delta x\epsilon\Delta\Omega}, \quad (2)$$

where Y is the number of detected neutrons, ϵ is the absolute efficiency of a neutron detector, $\Delta\Omega$ is the solid angle fraction subtended by a neutron detector, I is the number of particles that strikes the target with thickness Δx , and n is the nuclei per unit volume. The quantity I is determined by the accumulated charge during the measurement time while $\eta\Delta x$ is given by

$$\eta\Delta x = \frac{PN_A\rho\Delta x}{M}, \quad (3)$$

where P is the isotopic abundance of target atoms in the prepared foil, N_A is Avogadro's number, M is the target molar mass, and $\rho\Delta x$ is the target areal mass density.

The absolute efficiencies of the neutron detectors were measured with a (d,n) reaction on a ^{27}Al stopping target at $E_d=7.44$ MeV and at 120° . The differential cross section of the outgoing particle was normalized to the corresponding one obtained with a fission chamber [15] using the same reaction under the same kinematic conditions. A fission chamber was chosen because the fission cross sections are accurately known for the uranium isotopes.

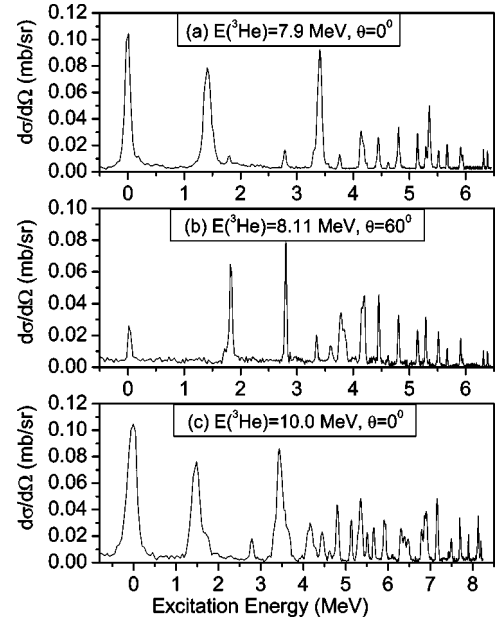


FIG. 4. Differential cross section per energy bin as a function of excitation energy for the $^{24}\text{Mg}(^3\text{He},n)^{26}\text{Si}$ reaction measurements. The bin width is given by Eq. (1).

The neutron detector efficiencies (including air and aluminum corrections) and the differential cross section spectra are shown in Figs. 3 and 4, respectively. The irregularities with minima and maxima in the absolute efficiency spectra are strongly correlated with resonances in the cross section

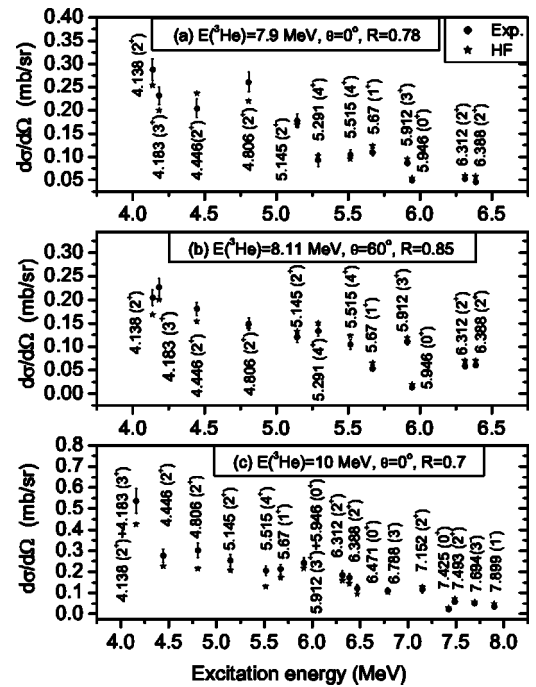


FIG. 5. Comparison of the experimental differential cross sections from the ^{26}Si measurements with the corresponding Hauser-Feshbach calculations. The sum of the differential cross sections for the 4.138(2^+)+4.183(3^+) and 5.912(3^+)+5.946(0^+) states are shown in (c) because they are not resolved in this measurement.

TABLE II. Optical model parameter (OMP) sets.

| OMP sets ^a | V_R | r_R | α_R | W_v | r_v | α_v | W_s | r_s | α_s | V_{so} | r_{so} | α_{so} | r_c |
|---|-----------------|-------|------------|--------------|-------|------------|--------------|-------|------------|----------|----------|---------------|-------|
| ²⁶ Si(n, n) | 48.9 | 1.28 | 0.7 | 0.0 | 0.00 | 0.0 | 12.3 | 1.28 | 0.4 | 4.5 | 1.08 | 0.7 | 0.0 |
| ²⁶ Al(p, p) | 51.6–0.21 E^b | 1.16 | 0.8 | 1.2+0.02 E | 1.40 | 0.7 | 4.2–0.03 E | 1.38 | 0.6 | 6.0 | 1.08 | 0.8 | 1.25 |
| ²³ Mg(α, α) | 126.6–0.24 E | 1.23 | 0.8 | 0.0 | 0.00 | 0.0 | 7.8+0.2 E | 1.58 | 0.6 | 0.0 | 0.00 | 0.0 | 1.23 |
| ²⁴ Mg(³ He, ³ He) | 177.0 | 1.10 | 0.7 | 28.8 | 1.20 | 0.7 | 0.0 | 0.0 | 0.0 | 0.0 | 0.00 | 0.0 | 1.2 |

^a V_i, W_i are in MeV and r_i, α_i in fm.

^b E is the incident kinetic energy in MeV.

for air and aluminum (scattering chamber) in the range of neutron energies of the present study. The 5% mass uncertainty of the highly enriched ²³⁵U fission chamber is included in the error propagation of the efficiencies and the differential cross sections. An additional 10% systematic uncertainty is assigned to the differential cross spectra due to the uncertainty in the target thickness. In Fig. 5 we show the measured differential cross sections for the states with $E_x > 4$ MeV.

Hauser-Feshbach calculations predict the angular distribution of the differential cross section of the emitted particles from the various exit channels of a compound nucleus. It takes into account the formation of the compound nucleus and the various residual nuclei of exit channels in states of different J^π and the level density in the region where compound nuclear levels overlap. The explicit expression for the Hauser-Feshbach (HF) differential cross section given by Douglas and McDonald [16] contains Racah and Clebsch-Gordan coefficients for angular momentum coupling, transmission factors to describe the probability for compound nucleus formation and decay, and spherical harmonics to describe the angular dependence. The HF code [17] is based on the theory and formulas in Ref. [18].

Transmission coefficients for (n, n), (p, p), (³He, ³He), and (α, α), particle separation energies, resolved levels, and level density parameters for the most probable exit channels were taken into consideration for the HF calculations of the ²⁷Si compound nucleus. The transmission coefficients were computed from the FOP code [19] which calculates the elastic cross sections. The optical model parameters were determined by a literature search and are listed in Table II. Level density parameters (a, σ, δ) were obtained by expressions derived by fitting experimental data and they are described in Ref. [20], while the known resolved levels and their J^π were taken from the NNDC [21]. Table III shows all energetically possible exit channels of neutrons, protons, alphas, or combinations of these. For some exit channels, we just needed resolved levels (RL) and for others resolved levels and level density parameters (RL+LDP) according to the maximum excitation energy of the residual nuclei.

The HF differential cross sections of every state were converted into the lab system, reduced, and compared with the experimental ones in Fig. 5. The HF results were reduced because the HF theory assumes that the cross sections in the nonelastic channels come entirely from the decay of the compound nucleus, so that only the elastic channels contribute in both direct (shape elastic) and compound processes [22]. In practice, however, there are frequently direct contributions to the nonelastic channels as well. This affects the

compound nucleus cross section even in channels with no direct component since the flux going into the direct nonelastic reactions does not enter the compound nucleus. Therefore, in the analysis of these interactions a reduction factor R should be defined. This reduction factor denotes the percentage of the reaction cross section which is compound. Lack of knowledge of all levels in every exit channel or low density parameter values could also lead to $R < 1$, while the opposite to $R > 1$. Five sets of level density parametric equations were built in the HF code related to analogous studies and provided the freedom to choose the appropriate level density parameters that match the experimental data best.

Figure 5 shows the comparison of the differential cross sections with the corresponding HF calculations, after the reduction, for every J^π state above 4 MeV in these measurements. States below 4 MeV were excluded since they had significant direct contribution. HF is sensitive to J but not to π changes; therefore our measurements can lead to a value for J but rely on other results for inferring π . A large number of levels especially at higher excitation energies had strengths consistent with HF calculations based on known spins (see Fig. 5). In several cases previous studies have reported two or three possible J^π values. In these cases we have adopted the assignment which gave the best agreement with HF calculations. All J^π assignments from this work in comparison with previous studies are listed in Table I, together with the excitation energy assignments discussed in the previous section. In the astrophysically important 5.9–6.0 MeV range the most recent studies [9,10] have indicated the presence of a 0^+ and a 3^+ state; older work [7] has suggested the possibility of a 4^+ state. In Fig. 6 we show the

TABLE III. Exit channels of the ²⁷Si compound nucleus for $E(^3\text{He})=10$ MeV.

| Open exit channels | $E_{\text{exc}}^{\text{max}}$ (MeV) | RL/LDP ^a |
|-------------------------------|-------------------------------------|---------------------|
| ²⁷ Si + γ | 22.00 | RL+LDP |
| ²⁶ Si + n | 8.69 | RL |
| ²⁶ Al + p | 14.54 | RL+LDP |
| ²⁵ Al + np | 3.17 | RL |
| ²⁵ Mg + $2p$ | 8.23 | RL |
| ²³ Mg + α | 12.66 | RL+LDP |
| ²² Na + αp | 5.20 | RL |
| ¹⁹ Ne + 2α | 3.32 | RL |

^aRL means that only the resolved levels up to $E_{\text{exc}}^{\text{max}}$ are needed while RL+LDP means that all the known resolved levels and the level density parameters are required.

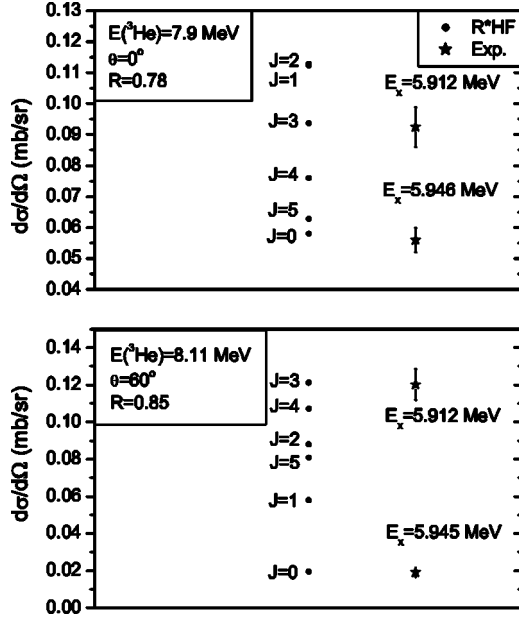


FIG. 6. Differential cross sections from Hauser-Feshbach calculations for states of $J=0-5$ in the excitation region of 5.9–6.0 MeV and the differential cross sections of the 5.192 and 5.946 MeV ^{26}Si from the $^{24}\text{Mg}(^3\text{He}, n)^{26}\text{Si}$ reaction measurements.

HF predicted cross sections for $0 \leq J \leq 5$ states in this excitation region along with our experimental data for the two low bombarding energy measurements. The comparison strongly favors 0^+ for the 5.946-MeV state. For the 5.912-MeV state we find $J^\pi=3^+$; a 4^+ assignment is only marginally consistent.

Some discussion of previous work in the context of our new results is in order. The early $^{24}\text{Mg}(^3\text{He}, n)^{26}\text{Si}$ experiment of Bohne *et al.* [7] was performed at higher energies than the present work (13.0 MeV) where direct reactions are expected to dominate and found a state at 5.910(30) MeV which had an angular distribution characteristic of a 0^+ state. In addition there was evidence for another L transfer which was interpreted as an indication of an unresolved 4^+ state. However given the uncertainties in the distorted-wave Born approximation calculations and the likely presence of multi-step and compound-nuclear processes this result could also arise from a 2^+ state or an unnatural parity state (see also the discussion in Ref. [10]). This interpretation is consistent with the present work which indicates a 3^+ state at 5.912(4) MeV and a 0^+ state at 5.946(4) MeV. The compilation of Endt [6] adopted J^π assignments based on the work of Bohne *et al.* The recent $^{28}\text{Si}(p, t)^{26}\text{Si}$ experiment of Bardayan *et al.* [9] found a state at 5.916(2) MeV. The authors claim to confirm the 0^+ assignment of Endt, but the DWBA calculation pre-

sented does not fit the data particularly well and importantly the experiment did not cover $\theta_{\text{c.m.}} < 20^\circ$ where the angular distribution for a 0^+ state is most unique. We believe that it is likely that this state corresponds to the 5.912-MeV state found in the present work which we find to have $J^\pi=3^+$. The recent $^{28}\text{Si}(^3\text{He}, ^6\text{He})^{26}\text{Si}$ measurements of Caggiano *et al.* [10] determined excitation energies for several levels in ^{26}Si including one at 5.945(8) MeV, consistent with the present work. However, we do not agree with their suggestion that this state has $J^\pi=3^+$. It should also be noted that the excitation energies found in the present experiment are in good agreement with Refs. [7,9,10] but are significantly lower than the excitation energies found by Paddock [8] in the 5–6.5 MeV range.

C. Astrophysical reaction rates

New astrophysical reaction rates were calculated for the $^{25}\text{Al}(p, \gamma)^{26}\text{Si}$ reaction based on the new location of the 3^+ resonance in this work. This is because of the sensitivity of the reaction rates to the resonance energy which differs by 33 keV from the corresponding value of Caggiano *et al.* [10].

The nonresonant and tail contribution rates are approximated by the same equation in Ref. [23] and their values are taken directly from Refs. [4,27] for temperatures ($T_9 = 0.03-1.5$) in explosive hydrogen burning environments. The resonance reaction rates of the $^{25}\text{Al}(p, \gamma)^{26}\text{Si}$ 3^+ ($\ell=0$) resonance and the two nearby states 1^+ ($\ell=2$) and 0^+ ($\ell=2$) resonances were calculated. These rates are approximated [23] as follows:

$$N_A \langle \sigma v \rangle_R = 1.5394 \times 10^{11} A^{-3/2} (\omega \gamma) T_9^{-3/2} \exp\left(-11.605 \frac{E_R}{T_9}\right), \quad (4)$$

where A is the reduced mass in amu, $\omega \gamma$ is the resonance strength in MeV, and E_R is the center-of-mass resonance energy in MeV. Proton and gamma widths were needed to calculate the resonance strength. The experimental values of the γ width of ^{26}Mg mirror states were used for the 3^+ and 0^+ states while a calculated value from Ref. [4] was used for the 1^+ state since the experimental value is only a lower limit. Proton widths were calculated based on the proportionality of the proton width to the penetrability [24], taking into account the penetrability ratio for the previous and new resonance energy location (i.e., assuming constant reduced width). Previous values for proton widths were taken from Ref. [4] where they were deduced from mirror states (neutron spectroscopic factors for states in ^{26}Mg have been determined using neutron-transfer experiments and/or shell-

TABLE IV. Parameters used in the astrophysical reaction rate calculations.

| E_x (MeV) | J^π | $E_r^{c.m.}$ (keV) | Γ_p (eV) | Γ_γ (eV) | $\omega \gamma$ (eV) |
|-------------|---------|--------------------|-----------------------|-----------------------|------------------------|
| 5.670 | 1^+ | 152 | 1.30×10^{-9} | 1.10×10^{-1} | 3.25×10^{-10} |
| 5.912 | 3^+ | 394 | 2.68×10^0 | 3.30×10^{-2} | 1.90×10^{-2} |
| 5.946 | 0^+ | 428 | 1.90×10^{-2} | 8.80×10^{-3} | 5.05×10^{-4} |

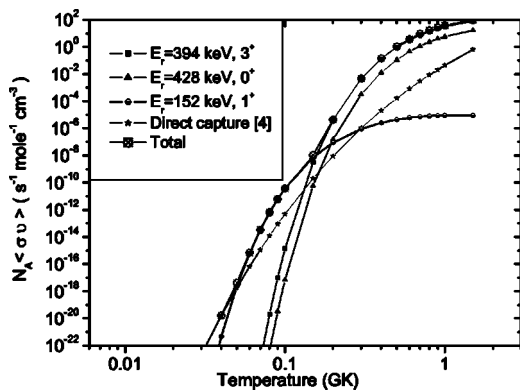


FIG. 7. Direct, resonant, and total rates for the $^{25}\text{Al}(p, \gamma)^{26}\text{Si}$ reaction.

model calculations). The penetrability of the Coulomb and centrifugal barrier is expressed in terms of the regular and irregular Coulomb wave functions [25] and was calculated using the PENE code [26]. Table IV shows the parameter values used in the reaction rate calculations and Fig. 7 presents these reaction rates as a function of the temperature range mentioned above. These rates are also listed in Table V. The figure includes the direct capture rate [4], the resonance reaction rates of the 3^+ , 1^+ , 0^+ states, and the total rates of the present study. As can be seen from Fig. 7, the $^{25}\text{Al}(p, \gamma)^{26}\text{Si}$ total rates are dominated by the two unnatural parity states (1^+ and 3^+) in the temperature range $T = 0.05 - 1.5$ GK. A comparison of the present total rates to the

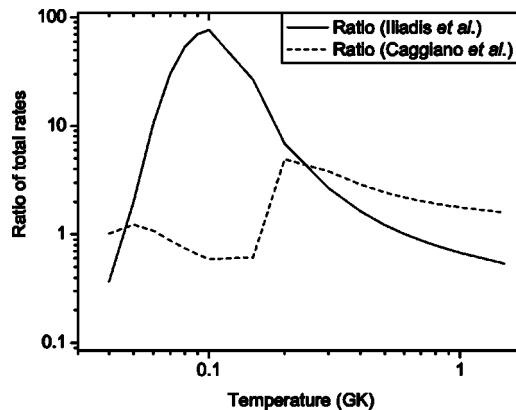


FIG. 8. Ratios of the present total rates to the corresponding rates of Iliadis *et al.* [4,27] and Caggiano *et al.* [10].

corresponding rates of Iliadis *et al.* [4,27] and Caggiano *et al.* [10] is shown in Fig. 8. The Caggiano *et al.* [10] total rates are closer to this work while both studies [4,10] show agreement with the present work at higher temperatures ($T > 0.2$ GK). The present increase of the reaction rates is the direct result of the change in resonance energy, because the resonance parameters (except the energies) were scaled from previous work.

IV. CONCLUSIONS

The $^{24}\text{Mg}(^3\text{He}, n)^{26}\text{Si}$ reaction was studied to deduce excitation energy values for the astrophysically important states

TABLE V. Stellar reaction rates $N_A \langle \sigma v \rangle$ (in $\text{s}^{-1} \text{mol}^{-1} \text{cm}^{-3}$) for $^{25}\text{Al}(p, \gamma)^{26}\text{Si}$.

| T (GK) | Direct capture ^a | Resonance ^b | Resonance ^c | Resonance ^d | Total |
|----------|-----------------------------|-------------------------|-------------------------|-------------------------|-------------------------|
| 0.03 | 2.100×10^{-23} | 2.972×10^{-28} | 3.847×10^{-61} | 1.977×10^{-67} | 2.100×10^{-23} |
| 0.04 | 1.590×10^{-20} | 4.674×10^{-22} | 8.819×10^{-45} | 1.215×10^{-49} | 1.636×10^{-20} |
| 0.05 | 1.770×10^{-18} | 2.263×10^{-18} | 5.354×10^{-35} | 5.310×10^{-39} | 4.033×10^{-18} |
| 0.06 | 6.410×10^{-17} | 6.160×10^{-16} | 1.694×10^{-28} | 6.263×10^{-32} | 6.801×10^{-16} |
| 0.07 | 1.120×10^{-15} | 3.259×10^{-14} | 7.186×10^{-24} | 6.799×10^{-27} | 3.371×10^{-14} |
| 0.08 | 1.190×10^{-14} | 6.225×10^{-13} | 2.067×10^{-20} | 3.958×10^{-23} | 6.344×10^{-13} |
| 0.09 | 8.720×10^{-14} | 6.045×10^{-12} | 9.924×10^{-18} | 3.287×10^{-20} | 6.132×10^{-12} |
| 0.1 | 4.840×10^{-13} | 3.664×10^{-11} | 1.362×10^{-15} | 6.998×10^{-18} | 3.712×10^{-11} |
| 0.15 | 2.040×10^{-10} | 7.136×10^{-9} | 3.085×10^{-9} | 5.906×10^{-11} | 1.048×10^{-8} |
| 0.2 | 9.110×10^{-9} | 8.766×10^{-8} | 4.087×10^{-6} | 1.510×10^{-7} | 4.335×10^{-6} |
| 0.3 | 1.040×10^{-6} | 9.026×10^{-7} | 4.540×10^{-3} | 3.237×10^{-4} | 4.860×10^{-3} |
| 0.4 | 2.040×10^{-5} | 2.549×10^{-6} | 1.331×10^{-1} | 1.320×10^{-2} | 1.463×10^{-1} |
| 0.5 | 1.680×10^{-4} | 4.407×10^{-6} | 9.370×10^{-1} | 1.131×10^{-1} | 1.050×10^0 |
| 0.6 | 8.350×10^{-4} | 6.036×10^{-6} | 3.272×10^0 | 4.507×10^{-1} | 3.724×10^0 |
| 0.7 | 2.980×10^{-3} | 7.290×10^{-6} | 7.713×10^0 | 1.167×10^0 | 8.883×10^0 |
| 0.8 | 8.520×10^{-3} | 8.176×10^{-6} | 1.428×10^1 | 2.319×10^0 | 1.661×10^1 |
| 0.9 | 2.060×10^{-2} | 8.754×10^{-6} | 2.259×10^1 | 3.874×10^0 | 2.648×10^1 |
| 1.0 | 4.400×10^{-2} | 9.093×10^{-6} | 3.205×10^1 | 5.744×10^0 | 3.784×10^1 |
| 1.5 | 6.310×10^{-1} | 8.910×10^{-6} | 8.011×10^1 | 1.637×10^1 | 9.711×10^1 |

^aFrom Ref. [4].

^bAt $E_r^{\text{c.m.}} = 152$ keV.

^cAt $E_r^{\text{c.m.}} = 394$ keV.

^dAt $E_r^{\text{c.m.}} = 428$ keV.

of the $^{25}\text{Al}(p, \gamma)^{26}\text{Si}$ reaction. The reaction measurements at 8 MeV provided adequate resolution to resolve these states that are located up to 1 MeV above the proton threshold in the ^{26}Si nucleus. The state at 5.912 MeV was assigned as a 3^+ resonance of the $^{25}\text{Al}(p, \gamma)^{26}\text{Si}$ based on the comparison between the measured differential cross section with HF calculations. New reaction rates were calculated based on these new assignments and they are presented in Fig. 7. In addition several states up to 7.9 MeV were located accurately and J^π were assigned to them (see Table I).

Confirmation of these excitation energies, spins, and parities would be desirable. Many J^π assignments for levels in ^{26}Si could be confirmed by measuring their γ -ray decays,

e.g., via $^{24}\text{Mg}(^3\text{He}, n\gamma)$. In addition direct determinations of the partial widths of the astrophysically relevant states would help to reduce uncertainties in the reaction rate. Higher bombarding energy measurements are also needed to complete the level structure of the ^{26}Si nucleus. It is hoped that in the future radioactive ^{25}Al beams will become another tool for the study of states above the proton threshold in ^{26}Si .

ACKNOWLEDGMENT

This work was supported by the U.S. DOE Grant No. DE-FG02-88ER40387.

-
- [1] R. Diehl, K. Bennett, H. Bloemen, H. de Boer, M. Busetta, W. Collmar, A. Connors, J. W. den Herder, C. de Vries, W. Hermesen, J. Knödelseder, L. Kuiper, G. G. Lichti, J. Lockwood, J. Macri, M. McConnell, D. Morris, R. Much, J. Ryan, V. Schönfelder, G. Simpson, J. G. Stacy, H. Steinle, A. W. Strong, B. N. Swanenburg, M. Varendorff, P. von Ballmoos, W. Webber, and C. Winkler, *Astron. Astrophys.* **97**, 181 (1993).
- [2] W. A. Mahoney, J. C. Ling, A. S. Jacobson, and R. E. Lingenfelder, *Astrophys. J.* **262**, 742 (1982).
- [3] G. H. Share, R. L. Kinzer, J. D. Kurfess, D. J. Forrest, E. L. Chupp, and E. Rigger, *Astrophys. J.* **292**, L61 (1985).
- [4] C. Iliadis, L. Buchmann, P. M. Endt, H. Herndl, and M. Wiescher, *Phys. Rev. C* **53**, 475 (1996).
- [5] R. D. Gehrz, J. W. Truran, R. E. Williams, and S. Starrfield, *Publ. Astron. Soc. Pac.* **110**, 3 (1998).
- [6] P. M. Endt, *Nucl. Phys.* **A521**, 192 (1990).
- [7] W. Bohne, K. D. Buchs, H. Fuchs, K. Grabisch, D. Hilscher, U. Jahnke, H. Kluge, T. G. Masterson, H. Morgenstern, and B. H. Wildenthal, *Nucl. Phys.* **A378**, 525 (1982).
- [8] R. A. Paddock, *Phys. Rev. C* **5**, 485 (1972).
- [9] D. W. Bardayan, J. C. Blackmon, A. E. Champagne, A. K. Dummer, T. Davinson, U. Greife, D. Hill, C. Iliadis, B. A. Johnson, R. L. Kozub, C. S. Lee, M. S. Smith, and P. J. Woods, *Phys. Rev. C* **65**, 032801(R) (2002).
- [10] J. A. Caggiano, W. Bradfield-Smith, R. Lewis, P. D. Parker, D. W. Visser, J. P. Greene, K. E. Rehm, D. W. Bardayan, and A. E. Champagne, *Phys. Rev. C* **65**, 055801 (2002).
- [11] R. W. Finlay, C. E. Brient, D. E. Carter, A. Marcinkowski, S. Mellema, G. Randers-Pehrson, and J. Rapaport, *Nucl. Instrum. Methods Phys. Res.* **198**, 197 (1982).
- [12] D. E. Carter and G. Randers-Pehrson, *Nucl. Instrum. Methods Phys. Res.* **199**, 497 (1982).
- [13] C. A. Baker, C. J. Batty, and L. E. Williams, *Nucl. Instrum. Methods* **59**, 125 (1968).
- [14] R. A. I. Bell, J. L'ecuyer, R. D. Gill, B. C. Robertson, I. S. Towner, and H. J. Rose, *Nucl. Phys.* **A133**, 337 (1969).
- [15] T. N. Massey, S. Al-Quraishi, C. E. Brient, J. F. Guillemette, S. M. Grimes, D. Jacobs, J. E. O'Donnell, J. Oldendick, and R. Wheeler, *Nucl. Sci. Eng.* **129**, 175 (1998).
- [16] A. C. Douglas and N. McDonald, *Nucl. Phys.* **13**, 382 (1959).
- [17] S. M. Grimes, Ohio University Report INPP-04-01 (unpublished).
- [18] S. M. Grimes, J. D. Anderson, J. W. McClure, B. A. Pohl, and C. Wong, *Phys. Rev. C* **10**, 2373 (1974).
- [19] F. S. Dietrich, LLNL report, 1983 (unpublished).
- [20] S. I. Al-Quraishi, S. M. Grimes, T. N. Massey, and D. A. Resler, *Phys. Rev. C* **67**, 015803 (2003).
- [21] National Nuclear Data Center, BNL, www.nndc.bnl.gov
- [22] P. E. Hodgson, *Nuclear Reactions and Nuclear Structure* (Clarendon Press, Oxford, 1971).
- [23] C. Angulo *et al.*, *Nucl. Phys.* **A656**, 3 (1999).
- [24] C. E. Rolfs and W. S. Rodney, *Cauldrons in the Cosmos* (University of Chicago Press, Chicago, 1988).
- [25] C. Iliadis, *Nucl. Phys.* **A618**, 166 (1997).
- [26] C. Iliadis (private communication).
- [27] C. Iliadis, J. M. D'Auria, S. Starrfield, W. J. Thompson, and M. Wiescher, *Astrophys. J., Suppl. Ser.* **134**, 151 (2001).